17th World Conference on Earthquake Engineering, 17WCEE
Sendai, Japan - September 13th to 18th 2020
Paper N° C001592 (Abstract ID)
Registration Code: S-A01095

DYNAMIC NUMERICAL MODELLING OF THE SEISMIC RESPONSE OF THE SANTIAGO CITY, CHILE

C. Pastén[1], D. Pavez[2], M. Acevedo[3], S. Ruiz[4], R. Astroza[5]

[1] Assistant Professor, Department of Civil Engineering, University of Chile, cpasten@uchile.cl
[2] M.Sc. Student, Department of Civil Engineering, University of Chile, dpavezcarrillo@gmail.com
[3] M.Sc. Student, Department of Civil Engineering, University of Chile, miguel.acevedo@uchile.cl
[4] Associate Professor, Department of Geophysics, University of Chile, sruiz@uchile.cl
[5] Assistant Professor, Faculty of Engineering and Applied Sciences, Universidad de los Andes, rastroza@miuandes.cl

Abstract

The Santiago City is located in Central Chile on a sedimentary basin, whose seismic response is controlled by the properties and geomorphology of the shallower quaternary deposits, as well as the impedance contrast with the underlying geological formations, among other factors. In this study, we built three representative two-dimensional (2D) cross-sections across the Santiago Basin in order to examine their seismic response. The wave velocities of the shallower quaternary sediments were determined from local geophysical measurements and the depth of the sedimentary cover was constrained with available gravimetric models and the H/V spectral ratio (HVSR) method. The cross-sections span from north to south (NS cross-section), east to west (EW cross-section), and north-east to south-west (CD cross-section) from soft sediments of average shear wave velocity of the upper 30 m (V_{s30}) of 400 m/s in the north to stiff gravels of average V_{s30} of 880 m/s in the south. The average thickness of the sediments is nearly 200 m, but it can reach 600 m at several depocenters in the city. The representative cross-sections were used to perform dynamic numerical simulations using the finite-difference code 2DFD_DVS. The input ground motions are impulse signals polarized in the longitudinal, transverse, and vertical directions with respect to the cross-sections imposed inside the model domain at a depth of 5 km. In addition, the one-dimensional (1D) response of the cross sections were calculated to compare with the 2D seismic response. The numerical results show that the more pronounced differences between the 1D and 2D modelling are found in the softer sediments, which also tend to amplify the ground motions more than stiffer sediments, in terms of spectral amplification factors and ground motion duration.

Keywords: basin effects; seismic amplification; finite-difference method; HVSR

1. Introduction

The Santiago City (Fig. 1) concentrates more than 40% of the Chile's population, along with most of the critical infrastructure of the country. The city is located next to the subduction of the Nazca plate underneath the South American plate, where large earthquakes frequently occur [1]. Two large earthquakes affected the urban area of the Santiago city during the last decades: the 1985 Mw 8.0 Valparaiso and the 2010 Mw 8.8 Maule earthquakes. The Medvedev–Sponheuer–Karnik scale (MSK) intensities reported in the Santiago basin ranged between VI - VIII, which are believed to be mainly associated to the surface geology characteristics [2], [3].

The dynamic seismic response of the Santiago Basin has been studied with numerical and geophysical methods. Bonnefoy-Claudet et al. [4] measured single-station ambient seismic noise and calculated H/V spectral ratios (HVSR) that provided estimates of the deposits predominant frequencies in the softer western and northern soil deposits, but produced inconclusive results in the stiff gravelly and alluvial soils, deposited in the south and east zones of the Basin, because the obtained HVSR were mainly flat with amplitudes lower than 2. Pilz et al. [5] compared site response techniques using earthquake and ambient seismic noise data, finding that HVSR from ambient noise provide a lower bound in amplitude for site amplification, particularly at frequencies higher than the fundamental one. Pilz et al. [6] proposed a simple shear wave velocity (Vs) model for a small area in the central part of the basin (26×12 km^2) from the inversion of large amplitude HVSR, complemented with gravimetric estimates of the sediment cover thickness, as well as geological and geophysical constraints. This study found that the MSK intensities of the 1985 earthquake correlate with low values of the average shear wave velocity of the upper 30 m (V_{s30}) and thicker sedimentary covers. Pilz et al. [7] simulated strong ground motion in the Basin using the spectral element method (SEM), adopting a simplified two-layers model, with a Vs that increases linearly with depth for the soil sediments and a constant Vs for the bedrock. The study concluded that the simplified model is able to reproduce the amplitudes and durations recorded for a regional Mw 6.0 shallow crustal earthquake up to 1.8 Hz. Recently, [8], [9] have performed numerical simulations to investigate the effect of crustal seismicity associated to the active San Ramón fault in the seismic hazard of the Santiago City. Both studies adopted a simplified soil shear wave velocity models and depths of the sedimentary soils.

Numerical simulation of sedimentary basins help to quantify non-linear material behavior [10], aggravation factors because of 2D and 3D effects over 1D amplification [11], [12], the effect of source-to-site azimuth [13], and amplification due to edge effects [14], among other factors. In this study, we attempt to construct detailed geotechnical cross-sections of the Santiago basin to numerically evaluate their surface seismic response when subjected to simplified impulse seismic sources.

2. Seismotectonic and Geologic Framework

The tectonic evolution of Central Chile is controlled by the subduction of the oceanic Nazca plate underneath the continental South American plate, at least since the Jurassic [15]. The Santiago City was founded in a sedimentary basin west of the Andes Cordillera (Fig. 1), in a geomorphological unit known as Chilean Central Depression, whose basement is composed by Eocene to Early Miocene volcano-sedimentary rocks, later filled with Pleistocene–Holocene alluvial, fluvial, and pyroclastic deposits [16] at approximately 500 m above sea level. The sedimentary cover of the basin is relatively shallow and flat, with 200 m of average depth and three depocenters that reach approximately 600 m, one of which is in the north-eastern side and the other two in the south-west side of the basin [17], [18]. The coalescence of the Mapocho and Maipo rivers filled the Basin with alluvial sediments, known as the Santiago gravel, composed primarily of gravel and pebbles of high strength and stiffness [4], [6]. The north of the basin consists of softer fine-grained-soils that create a large impedance contrast with the basement rock. Towards the west of the basin, there are pyroclastic deposits, known as Pudahuel Ignimbrite, composed of rhyolitic tuffs that merge with northern fine-grained soils and the Santiago gravel towards the basin central part [19]. These deposits have variable thickness and stiffness [20]. On the other hand, the east part of the basin is filled with alluvial deposits that are composed of boulders, gravels, and fine-grained soils in intricate structures and dominated by mudflows and fans [21]. Fig. 1 shows a simplified

geological model in the vicinity of the Santiago Basin and shows the three analyzed cross sections (NS, EW, CD) across the quaternary deposits.

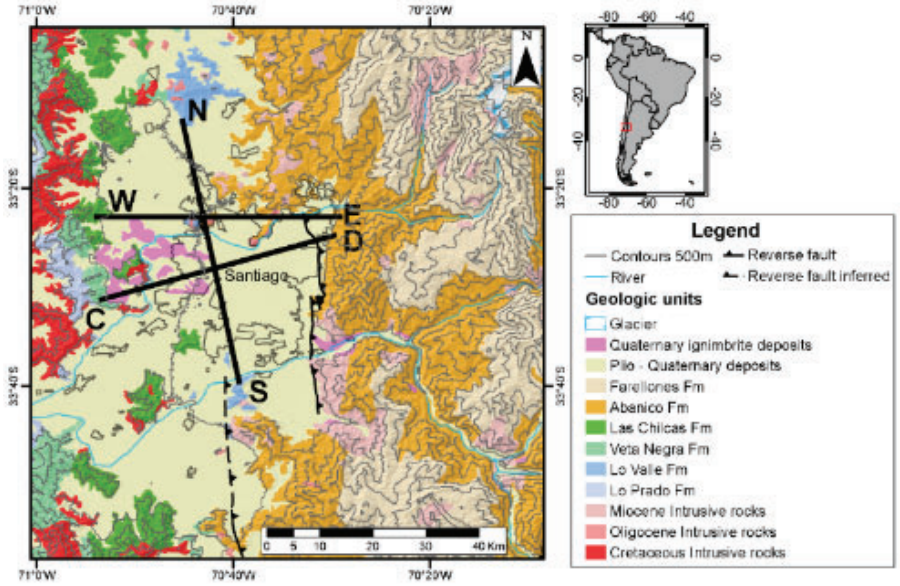

Fig. 1 – Simplified geological model in the vicinity of the Santiago Metropolitan Area. Black lines are the cross-sections analyzed in this study.

3. Cross-sections across the Santiago City

Fig. 2 shows the cross sections built and analyzed in this study. The depth of the bedrock is based on the gravimetric model proposed by Gonzalez et al. [17], whereas the details of plio-quaternary sediments are inferred from surface geology, geotechnical boreholes, shown in the figure, and shear wave velocity profiles measured with surface wave methods (not shown in the figure).

The cross-sections were used to perform dynamic numerical simulations using the finite-difference code 2DFD_DVS [22] (available at http://www.nuquake.eu). 2DFD_DVS allows simulating the 2D response of the cross-sections and the 1D responses of local soil columns in the cross-sections, assuming vertically propagating SH waves.

The constitutive model of all the involved materials is a generalized Maxwell model, modified by Emmerich & Korn (GMB-EK) [23]. Shear wave velocities of the materials were assigned as a function of depth z, following Eq. 1

$$V_s = V_{s0} + dV_s\sqrt{\frac{z}{1m}} \qquad \text{(m/s)} \tag{1}$$

Table 1 shows the specific values of the parameters V_{S0} and dV_S for each material in the cross-sections. The P-wave velocity was estimated according to [24] as

$$V_p = 1.11V_s + 1290 \qquad \text{(m/s)} \tag{2}$$

The attenuation factors for the S- and P-waves were estimated according to Eq. 3 and Eq. 4, respectively [12], [25], [26]

$$Q_s = \frac{V_s}{10} \tag{3}$$

$$Q_P = 2 \cdot Q_S \tag{4}$$

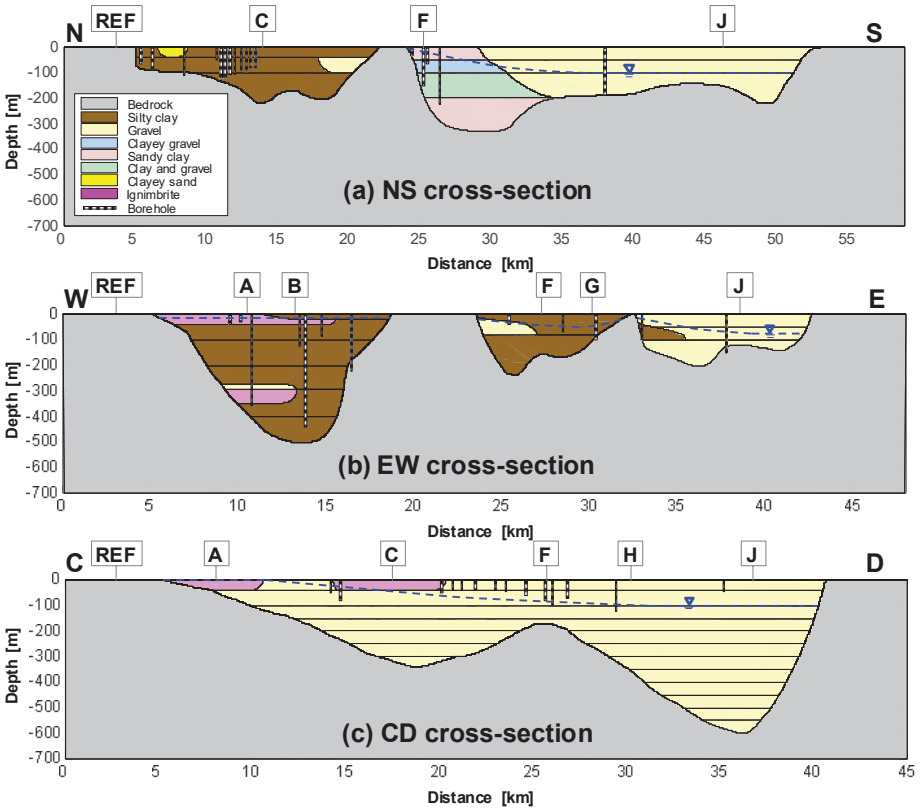

Fig. 2 – Analyzed geotechnical cross-sections of the Santiago Basin. (a) NS, (b) EW, and (c) CD cross-sections, shown in Fig. 1. The water table (dotted blue line) was inferred from [27].

We adopted the Gabor pulse as a simplified source function, similar to other studies (e.g., [28]–[30])

$$s(t) = exp\left\{-\left[\frac{\omega_p(t-t_s)}{\gamma_s}\right]^2\right\} cos\left[\omega_p(t-t_s)+\theta\right] \tag{5}$$

Where $\omega_p = 2\pi f_p$, $f_p = 0.18$ Hz, $\gamma_s = 0.2$ controls the temporal width of the signal, θ is a phase shift (disregarded in this model, θ=0°), and $t_s = 0.45\gamma_s/f_p = 0.5$ s. The Gabor signal runs from 0 to 1 s with a maximum amplitude at 0.5 s and has energy up to 5 Hz. This signal was input in the base of the cross-sections at 5 km depth. The polarization of the signal defines three independent two-dimensional (2D) models: (M1) P-SV model with a SV-wave input signal (contained in the cross-section plane), (M2) SH model with a SH-wave input signal (perpendicular to the cross-section plane), and (M3) P-SV model with vertical P-wave input signal. Models M1 and M3 have longitudinal and vertical components of motion, whereas model M2 has only a transverse component of motion. In addition, a fourth one-dimensional (1D) model (M4) was implemented, similar to model M2 with a SH-wave input signal, in order to compare the 2D and 1D responses.

Table 1 – Material parameters

Soil type	V_{S0} (m/s)	dV_S (m/s)	V_{S30} (1) (m/s)	Density (kg/m^3)
Silty clay	300	30	400	1600
Gravel	700	50	880	2100
Clayey gravel	400	55	600	2100
Sandy clay	400	55	600	1800
Clay and gravel	400	55	600	2000
Clayey sand	400	55	600	1900
Ignimbrite	300	14	350	1200
Bedrock (2)	2600	0	-	2600

Note: (1) V_{S30} was calculated analytically from Eq. 1; (2) bedrock V_p = 4500 m/s

4. Results

4.1 Surface ground motion

Fig. 3 shows the transverse component of motion at the surface of the cross-sections for an incident SH-wave (models M2 and M4). The upper panels of the figure show the results of 1D simulations from model M4 at surface points of the cross-sections separated 100 m between each other, and the lower panels show the results of model M2 at the same points. 1D and 2D simulations in the profiles show that the fine-grained soils, such as silty clay, sandy clay, clay sand, and ignimbrite soils, have larger and longer surface motion than the gravel soil. The main difference between the results of 1D and 2D simulations is the longer duration of the strong motion in fine-grained soil deposits due to the generation of surface waves at the boundaries of the soil deposits in the rock outcrops. These surface waves are more evident in the north side of the NS cross-section and west and center parts of EW cross-section. The difference between 1D and 2D modeling in gravel soils is negligible.

Fig. 4 shows the particle velocity of selected points at the surface of the cross-sections when subjected to SV- and SH-waves in 2D (models M1 and M2), and SH-wave in 1D (model M4). The figure confirms the results in Fig. 3, i.e., 2D simulations result in longer ground shaking in softer soils (Site C in NS cross-section and Sites A and F in EW cross-section) than the 1D simulation. This effect is less pronounced in sites over gravel soils (Sites J in NS, EW, and CD cross-sections and Site F in CD cross-section). The largest velocity amplitude in the figure is the one of Site C in the CD cross-section, where a shallower layer of ignimbrite of 50 m thick overlies the stiffer gravel. The large impedance contrast near the surface of the model may cause the wave front to amplify more than the other sites. This observation is confirmed from standard spectral ratios analyzed in the following sections.

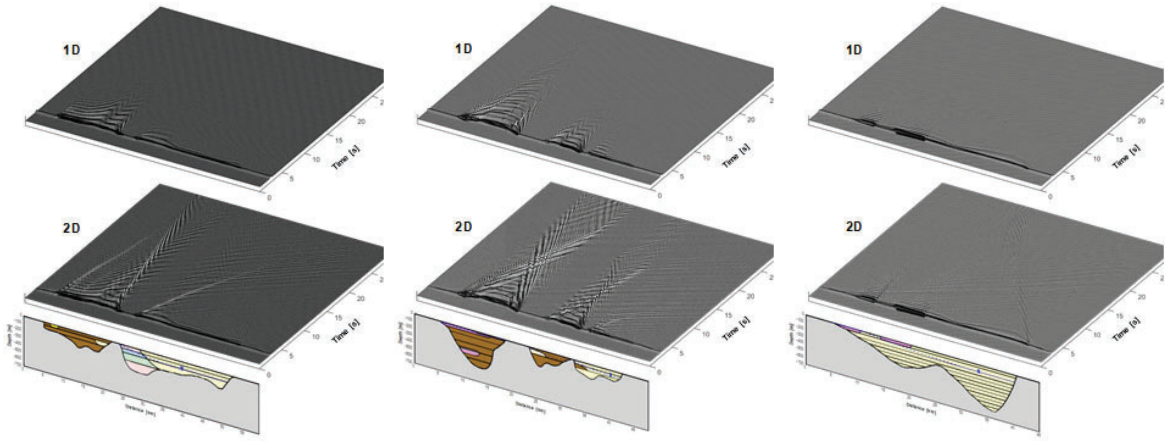

(a) (b) (c)

Fig. 3 – Transverse component of motion at the surface of the (a) NS, (b) EW, and (c) CD cross-sections for an incident SH-wave. Upper panels are the results of 1D models (M4) and lower panels are those of the 2D models (M2).

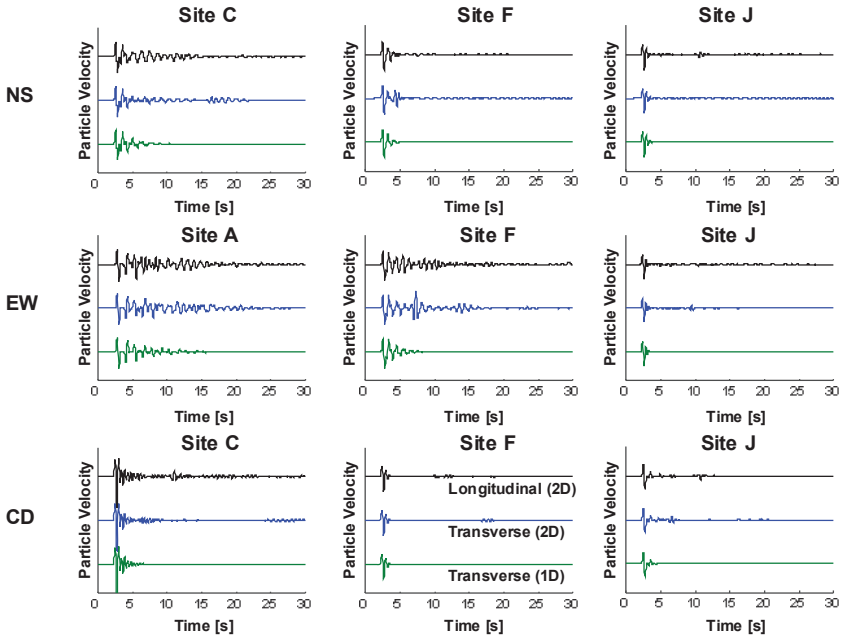

Fig. 4 – Particle velocity of selected points at the surface of the cross-sections subjected to SV and SH-waves in 2D (models M1 and M2), and SH-wave in 1D (model M4).

4.2 Standard spectral ratios

Fig. 5 shows standard spectral ratios (SSR) calculated as the ratio between the Fourier spectral amplitude of the surface velocity at selected surface sites and the Fourier spectral amplitude of the velocity at the reference site of each cross-section, indicated as REF in Fig. 2. The longitudinal SSR was computed from the longitudinal motion in model M1 (2D), the transverse SSR was computed from the transverse motion in model M2 (2D), and the vertical SSR was computed from the vertical motion in model M3 (2D). For comparison, Fig. 5 also depicts the transverse SSR computed from the transverse motion in model M4 (1D). The results in

the NS cross-section indicate that the longitudinal and transverse SSRs of 2D models amplify at the same resonant frequencies in Site C over silty clay soil (0.81; 2.2; 3.3; and 4.8 Hz), whereas the vertical component in the site amplifies at a higher frequency (2.4 Hz). The same outcome is observed in Site J over gravel, but the fundamental frequency is higher and the amplification is lower than that observed in Site C. In both sites, the longitudinal and transverse SSR of 2D models coincide well with the transverse SSR of the 1D model. Fig. 5 also shows SSRs for sites in the EW and CD cross-sections. The peak frequencies in the SSR are inversely proportional to the sediments thickness. For instance, Site A in the CD cross-section has a higher peak frequency at f = 2.2 Hz since the sediment thickness is only about H = 50m. In contrast, Site G in the EW cross-section has a lower peak frequency at f = 1 Hz due to the thicker soft soil layer (H = 100m).

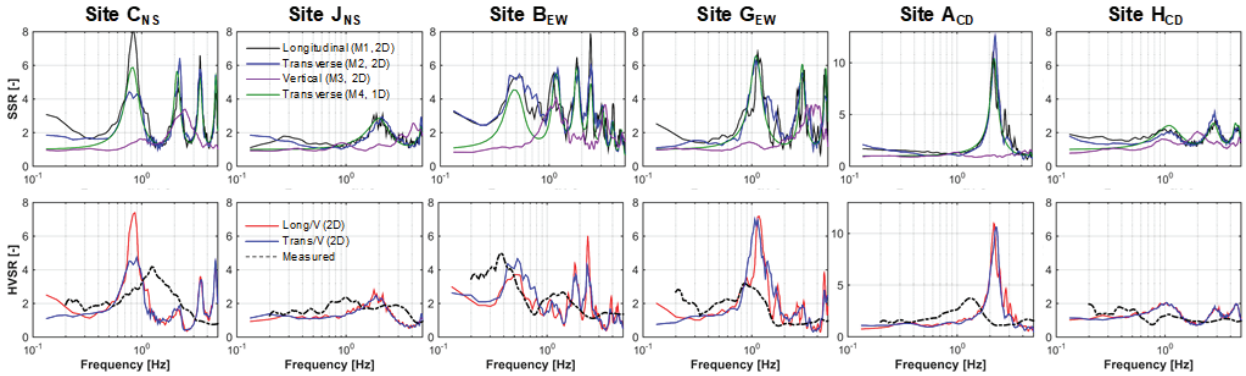

Fig. 5 – Standard spectral ratios (SSR) and H/V spectral ratios (HVSR) of selected sites in the NS, EW, and CD cross-sections. The curves with dotted lines in the lower panels are in-situ measured HVSRs. Sites locations are shown in Fig. 2.

4.3 H/V spectral ratios

H/V spectral ratios (HVSR) shown in Fig. 5 were obtained dividing the horizontal spectral amplitude of the longitudinal and transverse motion of models M1 and M2, respectively, by the vertical spectral amplitude obtained from model M3. The results in Fig. 5 show that HVSR retain similar features than the SSR, in terms of peak frequencies and amplitude, in all the analyzed sites. Recorded HVSR are plotted along with simulated HVSR in Fig. 5. The numerical predominant frequencies and amplitudes tend to be overestimated by the numerical simulations.

4.4 Predominant vibration frequencies

The peak predominant frequencies obtained from HVSR along the NS and EW cross-sections are summarized in Fig. 6. The figure compares simulated (diamonds) and measured predominant frequencies (filled symbols). Measured and simulated peak frequencies increase in the vicinity of the rock outcrops, and the simulated frequencies tend to be larger than the measured ones along the NS cross-section. Over the gravel sediments, the measured peak frequencies are not reported because the HVSR curves are flat and the peak amplitudes are lower than 2 (asterisks in Fig. 6). Measured and simulated peak frequencies in the EW cross-section coincide relatively well, except over the gravel soils, as described in the NS cross-section.

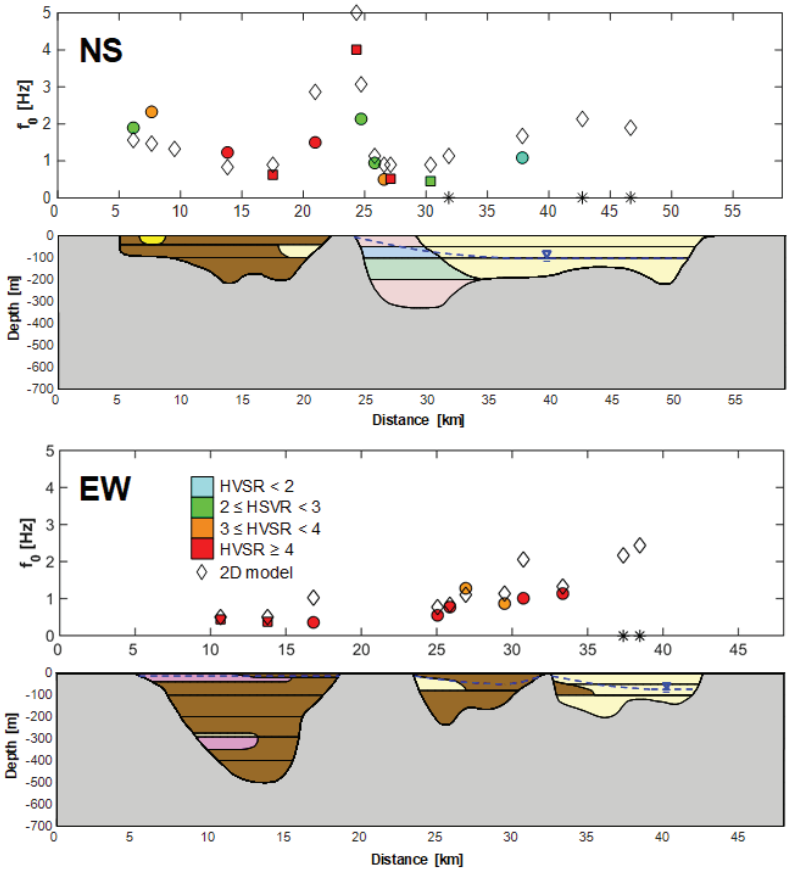

Fig. 6 – Peak predominant frequencies from HVSR along the NS and EW cross-sections. Filled symbols are recorded HVSR and open diamonds are simulated values.

4.5 Relative peak ground velocity

Fig. 7 and Fig. 8 show the peak ground velocities (PGV) simulated along the cross-sections with 1D and 2D models normalized by the PGV at a reference site in each of the cross-sections (reference sites shown in Fig. 2). The relative transverse PGV from the 1D and the 2D models, M4 and M2, respectively, are almost identical. Moreover, these values are similar to the relative longitudinal PGV from the 2D model M1. As expected, the larger amplification in terms of PGV is found over soft sediments in the NS and EW cross-sections. Also, a large amplification is predicted over the ignimbrites overlying gravelly soils in the CD cross-section. This amplification can be due to the large impedance contrast near the surface.

4.6 Spectral aggravation factor

We calculated a spectral aggravation factor (SAF) as a measure of the 2D amplification with respect to 1D seismic response. The SAF at a distance x from the reference site in each cross-section is calculated as the maximum value of the ratio between the response spectra obtained from transverse response of the 2D model M2 $SA_{2D}(x)$ and that obtained from the 1D model M4 $SA_{1D}(x)$, i.e.,

$$SAF(x) = max\left[\frac{SA_{2D}(x)}{SA_{1D}(x)}\right] \quad (6)$$

Fig. 7 and Fig. 8 show SAF along the three cross-sections, indicating that the spectral response of stiff gravel sediments in 1D and 2D are similar and close to unity, which is not the case for softer sediments where the 2D models amplifies more than the 1D model, reaching SAF as high as 2.

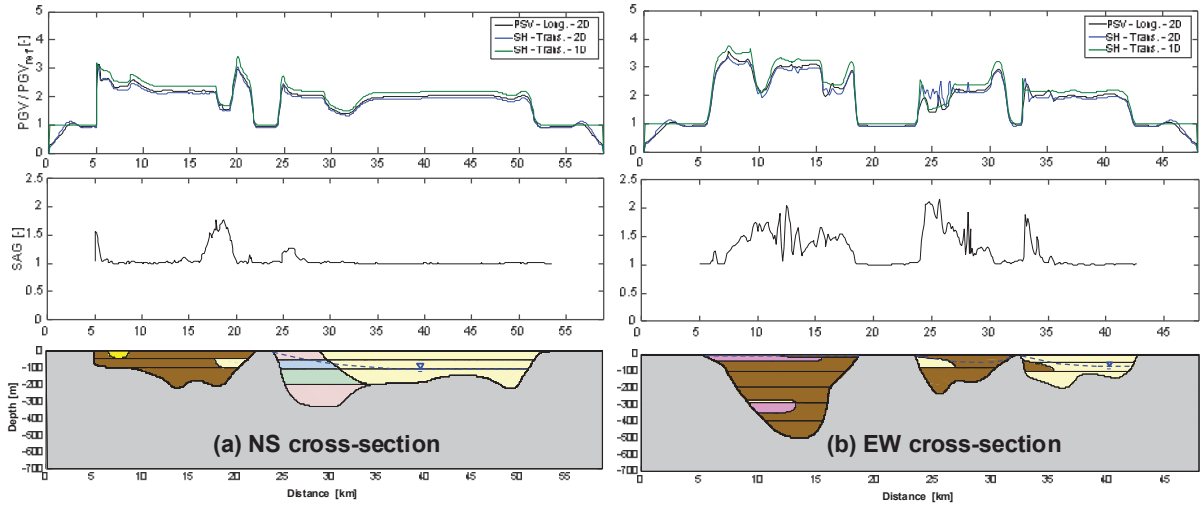

Fig. 7 – Relative peak ground velocity and spectral aggravation factor (SAF) along the (a) NS and (b) EW cross-sections.

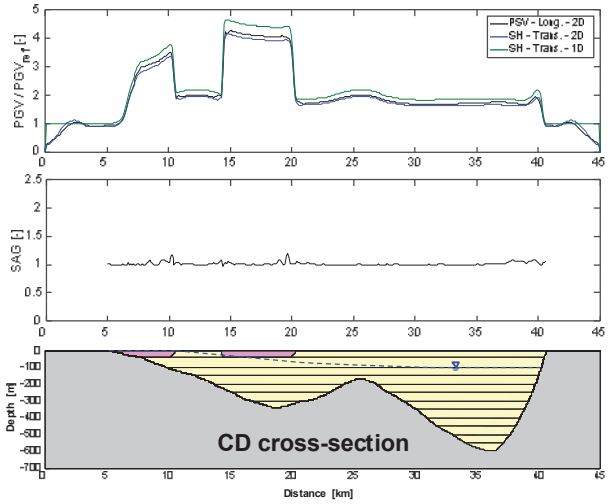

Fig. 8 – Relative peak ground velocity and spectral aggravation factor (SAF) along the CD cross-section.

5. Conclusions and final comments

The SSR from 2D and 1D simulations are similar; however, the velocity time histories show differences in the duration of the strong ground motion. The longer shaking in 2D models are due to surface waves generated at the boundaries of the sedimentary soils in the rock outcrops.

We found similarities in predominant frequencies and amplitudes between numerical SSR and HVSR. However, the numerical HVSR do not match the measured curves. In general, numerical results tend to overestimate the predominant frequencies which can be due to the high velocities with depth that we adopted for the materials.

The amplification of PGV from the 1D and the 2D models along the cross-sections are almost identical and the larger PGV amplification is found over soft sediments in the NS and EW cross-sections, particularly over the ignimbrites overlying gravelly soils in the CD cross-section.

Spectral aggravation factors in the three cross-sections show that the spectral response of stiff gravel sediments in 1D and 2D are similar (SAF≈1), whereas the 2D response of softer sediments can double the 1D response.

6. Acknowledgements

Support for this research was provided by the Conicyt Fondecyt grant N°1190995 and the National Laboratory for High Performance Computing (NLHPC). César Pastén thanks the support from the Advanced Mining Technology Center (AMTC FB0809 PIA CONICYT).

7. References

[1] S. Ruiz and R. Madariaga, "Historical and recent large megathrust earthquakes in Chile," *Tectonophysics*, vol. 733, no. December 2017, pp. 37–56, 2018.

[2] F. Leyton *et al.*, "Seismic Zonation of the Santiago Basin, Chile," *5th Int. Conf. Earthq. Geotech. Eng.*, 2011.

[3] M. Astroza, S. Ruiz, and R. Astroza, "Damage assessment and seismic intensity analysis of the 2010 (Mw 8.8) maule earthquake," *Earthq. Spectra*, vol. 28, no. SUPPL.1, pp. 145–164, 2012.

[4] S. Bonnefoy-Claudet *et al.*, "Site effect evaluation in the basin of Santiago de Chile using ambient noise measurements," *Geophys. J. Int.*, vol. 176, no. 3, pp. 925–937, 2009.

[5] M. Pilz, S. Parolai, F. Leyton, J. Campos, and J. Zschau, "A comparison of site response techniques using earthquake data and ambient seismic noise analysis in the large urban areas of Santiago de Chile," *Geophys. J. Int.*, vol. 178, no. 2, pp. 713–728, 2009.

[6] M. Pilz *et al.*, "Shear wave velocity model of the Santiago de Chile basin derived from ambient noise measurements: A comparison of proxies for seismic site conditions and amplification," *Geophys. J. Int.*, vol. 182, no. 1, pp. 355–367, 2010.

[7] M. Pilz, S. Parolai, M. Stupazzini, R. Paolucci, and J. Zschau, "Modelling basin effects on earthquake ground motion in the Santiago de Chile basin by a spectral element code," *Geophys. J. Int.*, vol. 187, no. 2, pp. 929–945, 2011.

[8] M. Cortés, "3D Physics-based numerical scenarios for earthquake strong ground motion prediction: The case of the San Ramón fault in Santiago de Chile Basin," Politecnico Milano, 2018.

[9] J.-B. Ammirati *et al.*, "The Crustal Seismicity of the Western Andean Thrust (Central Chile, 33°–34° S): Implications for Regional Tectonics and Seismic Hazard in the Santiago Area," *Bull. Seismol. Soc. Am.*, vol. 109, no. 5, pp. 1985–1999, 2019.

[10] G. Falcone, D. Boldini, and A. Amorosi, "Site response analysis of an urban area: A multi-dimensional and non-linear approach," *Soil Dyn. Earthq. Eng.*, vol. 109, no. February, pp. 33–45, 2018.

[11] P. Moczo *et al.*, "Key structural parameters affecting earthquake ground motion in 2D and 3D sedimentary structures," *Bull. Earthq. Eng.*, 2018.

[12] C. Zhu, E. Riga, K. Pitilakis, J. Zhang, and D. Thambiratnam, "Seismic Aggravation in Shallow Basins in Addition to One-dimensional Site Amplification," *J. Earthq. Eng.*, vol. 00, no. 00, pp. 1–23, 2018.

[13] E. A. Wirth *et al.*, "Source-Dependent Amplification of Earthquake Ground Motions in Deep Sedimentary Basins," *Geophys. Res. Lett.*, vol. 46, no. 12, pp. 6443–6450, 2019.

[14] C. Zhu, F. J. Chávez-García, D. Thambiratnam, and C. Gallage, "Quantifying the edge-induced seismic aggravation in shallow basins relative to the 1D SH modelling," *Soil Dyn. Earthq. Eng.*, vol. 115, no. November 2016, pp. 402–412, 2018.

[15] C. Mpodozis and V. Ramos, "The Andes of Chile and Argentina," 1990.

[16] D. Sellés and P. Gana, "Geología del área Talagante-San Francisco de Mostazal: región metropolitana de Santiago y del Libertador general Bernardo O'Higgins," Servicio Nacional de Geología y Minería, 2001.

[17] F. A. González *et al.*, "Characterization of the depocenters and the basement structure, below the central Chile Andean Forearc: A 3D geophysical modelling in Santiago Basin area," *Basin Res.*, vol. 30, no. 4, pp. 799–815, 2018.

[18] G. Yañez, M. Muñoz, V. Flores-Aqueveque, and A. Bosch, "Gravity derived depth to basement in Santiago Basin, Chile: implications for its geological evolution, hydrogeology, low enthalpy geothermal, soil characterization and geo-hazards," *Andean Geol.*, vol. 42, no. 2, pp. 147–172, 2015.

[19] C. R. Stern, H. Amini, R. Charrier, E. Godoy, F. Herve, and J. Varela, "Petrochemistry and age of rhyolitic pyroclastic flows which occur along the drainage valleys of the Rio Maipo and Rio Cachapoal (Chile) and the Rio Yaucha and Rio Papagayos (Argentina)," *Rev. Geológica Chile*, no. 23, pp. 39–52, 1984.

[20] S. Rebolledo, J. Lagos, R. Verdugo, and M. Lara, "Geological and geotechnical characteristics of the Pudahuel ignimbrite , Santiago , Chile," *Geol. Soc. London IAEG*, no. 106, pp. 1–10, 2006.

[21] R. Armijo *et al.*, "The West Andean Thrust, the San Ramón Fault, and the seismic hazard for Santiago, Chile"," *Tectonics*, vol. 29, no. 4, pp. 1–34, 2010.

[22] P. Moczo, J. Kristek, M. Galis, P. Pazak, and M. Balazovjech, "The finite-difference and finite-element modeling of seismic wave propagation and earthquake motion," *Acta Phys. Slovaca*, vol. 57, no. 2, pp. 177–406, 2007.

[23] H. Emmerich and M. Korn, "Incorporation of attenuation into time-domain computations of seismic wave fields," *Geophysics*, vol. 52, no. 9, pp. 1252–1264, 1987.

[24] C. Kitsunezaki *et al.*, "Estimation of P- and S- wave velocities in deep soil deposits for evaluating ground vibrations in earthquake," *J. Japan Soc. Nat. Disaster Sci.*, vol. 9, pp. 1–17, 1990.

[25] E. Maufroy *et al.*, "3D numerical simulation and ground motion prediction: Verification, validation and beyond – Lessons from the E2VP project," *Soil Dyn. Earthq. Eng.*, vol. 91, no. February, pp. 53–71, 2016.

[26] E. Riga, K. Makra, and K. Pitilakis, "Aggravation factors for seismic response of sedimentary basins: A code-oriented parametric study," *Soil Dyn. Earthq. Eng.*, vol. 91, no. February, pp. 116–132, 2016.

[27] M. Muñoz *et al.*, "Estimating low-enthalpy geothermal energy potential for district heating in Santiago basin e Chile (33 . 5 S)," vol. 76, pp. 186–195, 2015.

[28] F. J. Chávez-García, "Site effects in Parkway Basin: Comparison between observations and 3-D modelling," *Geophys. J. Int.*, vol. 154, no. 3, pp. 633–646, 2003.

[29] J. Kristek, P. Moczo, P.-Y. Bard, F. Hollender, and S. Stripajová, "Computation of amplification factor of earthquake ground motion for a local sedimentary structure," *Bull. Earthq. Eng.*, 2018.

[30] L. Lenti and S. Martino, "The interaction of seismic waves with step-like slopes and its influence on landslide movements," *Eng. Geol.*, vol. 126, pp. 19–36, 2012.